Neuropharmacology 300 (2026) 111152

Contents lists available at ScienceDirect

Neuropharmacology

journal homepage: www.elsevier.com/locate/neuropharm

Targeted optical uncaging of an adenosine A_1 receptor agonist regulates excitability of hippocampal slices derived from epileptic mice

Marijke Vergaelen [a,*], Kristl Vonck [a], Ruben Tack [b], Melissa Lajtos [a,c], Simona Manzella [a], Jeroen Missinne [d], Mathieu Sprengers [a], Evelien Carrette [a], Paul Boon [a], Serge Van Calenbergh [b], Robrecht Raedt [a]

[a] 4BRAIN, Department of Head and Skin, Ghent University, Belgium
[b] Laboratory of Medicinal Chemistry, Ghent University, Belgium
[c] IBME-MEDISIP, Department of Electronics and Information Systems, Ghent University, Belgium
[d] Center for Microsystems Technology, Ghent University and Imec, Belgium

ARTICLE INFO

Keywords:
Photopharmacology
Adenosine
Epilepsy
Neuromodulation
(MEA)Multielectrode array
Hippocampus
Field potentials

ABSTRACT

Photocaged adenosine A_1 receptor (A_1R) agonists combined with spatiotemporally selective illumination represents a promising therapeutic strategy for mesial temporal lobe epilepsy (mTLE). This *ex vivo* study investigated whether the A_1R agonist N^6-cyclopentyladenosine (CPA) suppresses hippocampal excitability in the intrahippocampal kainic acid (IHKA) mouse model and whether photocaged CPA (cCPA) enables subregion-selective and closed-loop reduction of hippocampal excitability.

Hippocampal slices from male IHKA and saline-injected control mice were exposed to CPA (10-900 nM) while electrically evoked field postsynaptic potentials (fPSPs) were recorded in dentate gyrus (DG) and CA1. We evaluated fPSP slope (neurotransmission strength) and population spike (PS) amplitude (postsynaptic activation). Next, hippocampal slices were superfused with 3 μM cCPA while focally illuminating DG or CA1 to investigate spatial targeting. Finally, a cCPA-based closed-loop system was tested to maintain PS amplitude at 50% of baseline.

While CPA-induced fPSP slope reduction was similar in CA1 between IHKA and control slices, it was significantly reduced in DG for IHKA compared to control slices. This difference was absent when extracellular K^+ was increased from 3.25 mM to 5.5 mM. In 5.5 mM K^+, CPA similarly decreased excitability in DG and CA1 in IHKA and control slices. Focal CPA photorelease inhibited neurotransmission with limited effects in non-illuminated regions, indicating subregion-selective inhibition. Closed-loop control stabilized DG PS amplitude at the predefined level in IHKA slices.

Adenosine A_1R activation robustly reduces excitability in the hippocampus from IHKA mice. Photopharmacology enables spatially controlled and closed-loop inhibition to maintain stable DG output, offering a targeted treatment strategy for mTLE.

1. Introduction

Despite the availability of numerous antiseizure medications (ASMs) with various mechanisms of action, up to 60% of patients with mesial temporal lobe epilepsy with hippocampal sclerosis (mTLE-HS) remain drug-resistant (Kalilani et al., 2018; Bjørke et al., 2018). A significant limitation in conventional pharmacological treatment is the lack of spatiotemporal precision. As systemic ASMs not only affect their targets at intended sites but also other organ systems, including the whole central and peripheral nervous system, they often cause dose-limiting side effects (Androsova et al., 2017). Furthermore, the continuous administration of ASMs contrasts with the paroxysmal nature of seizures. Improving efficacy and spatiotemporal precision in seizure management, could be obtained by closed-loop photopharmacology. In this dual approach, photopharmacology provides spatial control by restricting drug action to targeted brain regions, while a closed-loop system provides temporal control by continuously monitoring neuronal activity and triggering photopharmacological intervention

* Corresponding author.
E-mail addresses: Marijke.Vergaelen@UGent.be, marijke_vergaelen@hotmail.com (M. Vergaelen).

https://doi.org/10.1016/j.neuropharm.2026.111152
Received 19 June 2026; Received in revised form 12 August 2026; Accepted 14 August 2026
Available online 17 August 2026
0028-3908/© 2026 The Authors. Published by Elsevier Ltd. This is an open access article under the CC BY license (http://creativecommons.org/licenses/by/4.0/).

only upon detecting hyperexcitability. Unlike an open-loop system, which delivers treatment according to a preprogrammed schedule regardless of real-time brain state, a closed-loop system dynamically adapts treatment delivery to match ongoing changes in neuronal excitability (Krook-Magnuson et al., 2015a).

The dentate gyrus (DG) represents a strategic target for this precision approach. Acting as the 'gatekeeper' for the hippocampus, the DG only sparsely transmits excitatory input to the rest of the hippocampal circuitry because the granule cells are difficult to excite: their resting membrane potential is more hyperpolarized, dendritic postsynaptic potentials are strongly attenuated and feedforward and feedback inhibition is extensive (Krueppel et al., 2011; Lee et al., 2016; Liu et al., 2014; Staley et al., 1992; Krook-Magnuson et al., 2015b). In mTLE-HS, the DG becomes hyperexcitable due to profound pathological reorganization, including the loss of GABAergic inhibition and a strong increase in interneuronal connectivity mostly due to mossy fibre sprouting (Krook-Magnuson et al., 2015b; Häussler et al., 2012; Hendricks et al., 2019; Scharfman, 2019). We previously demonstrated that this pathological increase in hippocampal excitability is mainly restricted to the DG in the intrahippocampal kainic acid (IHKA) mouse model, with the cornu ammonis (CA) 1 region maintaining its regular excitability levels (Vergaelen et al., 2024). Consequently, targeting neuronal inhibition to the dysfunctional hyperexcitable dentate gate may represent a therapeutic strategy for seizure control with minimal impact on other brain functions. We envisage a closed-loop system that (i) continuously probes excitability levels in the DG by measuring postsynaptic activation in response to electrically evoked afferent input (ii) locally releases ASM when postsynaptic activation exceeds a threshold, indicating hyperexcitability; and (iii) avoids excessive suppression of neurotransmission that would compromise physiological hippocampal functioning.

To achieve triggered release of ASM, we propose a photopharmacological approach using photocaged compounds. These molecules remain biologically inert until illumination triggers the release of the parent compound at the targeted site (Ganzoni et al., 2025). Our approach targets the adenosine A_1 receptor (A_1R), the primary mediator of the endogenous seizure-suppressive actions of adenosine, particularly given the diminished adenosinergic inhibitory tone characteristic of mTLE-HS (Spanoghe et al., 2021). Adenosine A_1R activation triggers $G_{i/o}$-mediated signalling, suppressing neurotransmission and neuronal excitability, primarily through the inhibition of voltage-gated Ca^{2+} channels (VGCCs) and the activation of G protein-coupled inwardly rectifying K^+ (GIRK) channels, respectively (Spanoghe et al., 2021; Borea et al., 2018a; Gouder et al., 2003; Tescarollo et al., 2020). While systemic administration of adenosine A_1R agonists results in potent seizure suppression, their clinical use is hindered by severe cardiovascular and sedative side effects (Gouder et al., 2003; Borea et al., 2018b; Schindler et al., 2005).

To investigate a photopharmacological approach targeting the adenosine A_1R signalling pathway, we previously developed a photocaged derivative of the adenosine A_1R agonist N^6-cyclopentyladenosine (CPA) by coupling it to a coumarin-based photocage (photocaged CPA, cCPA) (Craey et al., 2022). Using this compound, we demonstrated in an *in vivo* proof-of-concept study that intracerebroventricular (ICV) injection of cCPA followed by open-loop illumination (i.e. fixed light delivery) of the DG significantly suppressed electrically evoked field postsynaptic potentials (fPSPs) in healthy mice and spontaneous seizures in the IHKA mouse model (Spanoghe et al., 2025). Moreover, we evaluated a closed-loop approach in *ex vivo* settings. We superfused rat hippocampal slices with 3 μM cCPA (i.e. ~100x the EC_{50} of CPA) and recorded electrically evoked fPSPs every 10 s in CA1. Whenever the fPSP amplitude, reflecting the neurotransmission strength, surpassed a predefined threshold, the slice was exposed to milliseconds a flash of 405 nm light to release nanomolar concentrations of CPA, resulting in a reduction of neurotransmission strength, reflected by decreased fPSP amplitude (Craey et al., 2022, 2026). Applying this closed-loop photopharmacological approach in the high-K^+ hippocampal slice model allowed to keep neurotransmission at preset levels in the CA1 thereby controlling excitability and suppressing epileptiform bursting (Craey et al., 2026). Until now, the performance of our closed-loop approach in modulating the hyperexcitable DG under chronic epilepsy conditions remained to be investigated.

In the current study, we investigated the performance of closed-loop photopharmacology *ex vivo* in the DG of slices derived from epileptic IHKA mice to provide the basis for future *in vivo* closed-loop implementation. First, we evaluated to which degree the inhibitory effect of the adenosine A_1R pathway is affected by the pathophysiological changes in mTLE-HS by directly comparing CPA efficacy in hippocampal slices from IHKA versus control mice across both the DG and CA1 subregions. Second, we evaluated whether photopharmacological activation of the inhibitory adenosine A_1R-mediated signalling could be targeted to the hyperexcitable DG through illumination focused on hippocampal subregions (DG versus CA1). Third, we investigated whether closed loop photopharmacology could achieve sustained and stable suppression of postsynaptic activation within the hyperexcitable DG of IHKA mice.

2. Material and methods

2.1. Animals

Male C57Bl/6J mice (seven weeks of age) were purchased from Envigo (The Netherlands). Animals were group-housed at a controlled temperature of 20-22°C and at a relative humidity of 40-60% with a fixed 12 h light/dark cycle and food and water provided *ad libitum*. After intrahippocampal kainic acid (KA) injection, mice were single-housed to avoid severe aggressive behaviour. All experiments were conducted in accordance with the European guidelines (directive 2010/63/EU) and were approved by the Animal Experimental Ethical Committee of Ghent University (ECD19/65 and ECD 22/39).

2.2. Compounds

The adenosine A_1R agonist CPA was provided by Sigma-Aldrich (Catalog No. 1702, St. Louis, MO, USA). cCPA was produced according to our previously described protocol by Oxeltis (France) (Craey et al., 2022). Stock solutions of both compounds were prepared in 100% dimethylsulfoxide (DMSO, Catalog No.: 3176, Tocris Biosciences, UK) and subsequently diluted in artificial cerebrospinal fluid (aCSF) to the desired concentrations. The resulting final DMSO concentration was 0.1%. The standard used aCSF was composed of (in mM): 124 NaCl, 2 KCl, 1.25 KH_2PO, 2 $CaCl_2$, 2 $MgSO_4$, 26 $NaHCO_3$ and 10 glucose, which will be referred to as 3.25 mM K^+ aCSF. In one experiment, the KCl concentration was increased to 4.25 mM, resulting in a total K^+ concentration of 5.5 mM, which will be called 5.5 mM K^+ aCSF.

2.3. Intrahippocampal kainic acid injection and status epilepticus

Status epilepticus (SE) was induced in eight-weeks old mice (n = 63) via the injection of KA (200 ng diluted in 50 nL of saline) into the right dorsal hippocampus, further referred to as IHKA mice. In humans, SE is defined as an abnormally prolonged seizure (beyond 5 to 10 min depending on seizure type) that can result in long-term neuronal injury (Trinka et al., 2015). In the IHKA model, SE manifests immediately following KA injection as an non-convulsive or convulsive SE characterized electrographically by hippocampal paroxysmal discharges accompanied behaviourally by immobility, staring, and twitching which initiates hippocampal sclerosis and epileptogenesis. This results in spontaneous recurrent seizures from two weeks after KA injection (Riban et al., 2002). In this study, during the first hours after KA injections, frequent behavioural arrest and clonic seizures, indicative of SE, were observed visually. Nine mice died within the first hours post KA injection due to the SE. In our previous studies KA injection resulted in

electrophysiologically identifiable seizures recorded after four weeks and pathophysiological changes such as loss of CA1/CA3 pyramidal neurons and granule cell dispersion in dorsal and intermediate hippocampal regions (Spanoghe et al., 2025; Desloovere et al., 2019, 2021). A batch of non-epileptic mice (n = 27) were intrahippocampally injected with vehicle solution (50 nL of saline) or were not injected (n = 3) and served as controls. The saline-injected mice were used for direct comparisons to IHKA mice, while this was not the case for the healthy mice. This is highlighted in section '**2.6 Experimental protocols**'.

The injections were performed as described in previous work (Vergaelen et al., 2024). In summary, after anesthetizing the animals with isoflurane (induction 5%, maintenance 2%) and medical O_2 (induction 1 L/min, maintenance 0.8 L/min), they were secured in a stereotactic frame (Neurostar Robot Stereotaxic system, Neurostar, Tubingen, Germany) using ear bars. After exposing the skull and making a craniotomy, the injection was performed at a rate of 100 nL/min with a blunt tip needle (25 gauge) connected to a 1 μl Hamilton syringe (Hamilton, syringe ref. 65458, needle ref. 7001) in the dorsal hippocampus according to the following stereotactic coordinates: [AP] −2.0 mm relative to bregma; [ML] +1.5 mm relative to bregma; [DV] −1.8 mm relative to brain surface.

2.4. Hippocampal slice preparation

Four to eight weeks after intrahippocampal injection of KA or saline, mice were anaesthetised with 5% isoflurane before decapitation. Immediately following decapitation, the brain was rapidly extracted and submerged in ice-cold 3.25 mM K^+ aCSF. A stable pH of 7.4 was maintained by continuous aeration (95% O_2/5% CO_2). Horizontal cortico-hippocampal slices (350 μm thickness) were prepared using a Leica VT1200S vibratome (Leica Microsystems, Wetzlar, Germany) and placed in carbogen-saturated 3.25 mM K^+ aCSF at room temperature for at least 1 h until use. Only slices from the intermediate hippocampus ([DV] 2 - 3.75 mm relative to brain surface) were selected, excluding the injected dorsal hippocampus where high concentrations of KA caused massive neuronal death (Le Duigou et al., 2005, 2008).

For electrophysiological recordings, slices were transferred to the multielectrode array (MEA) chamber (MCS, Reutlingen, Germany) and continuously perfused with carbogen-saturated aCSF at a flow rate of 2 mL/min. Carbogen-saturated aCSF was preheated to 31°C in the superfusion cannula (PH01, MultiChannel Systems (MCS), Reutlingen, Germany). The temperature in the MEA chamber was maintained at 31°C. Slice position on top of the MEA electrodes was maintained with the help of a custom-made nylon grid. At least 15 min of equilibration time was provided before the start of the experiment.

2.5. Electrophysiological set-up and evoked potential recording

Field potentials were recorded with a planar 60 channel MEA (MCS, Reutlingen, Germany), containing 60 TiN-coated electrodes (30 μm diameter and 200 μm spacing), one of which is connected to the system's ground and used as reference electrode. Voltage signals were acquired

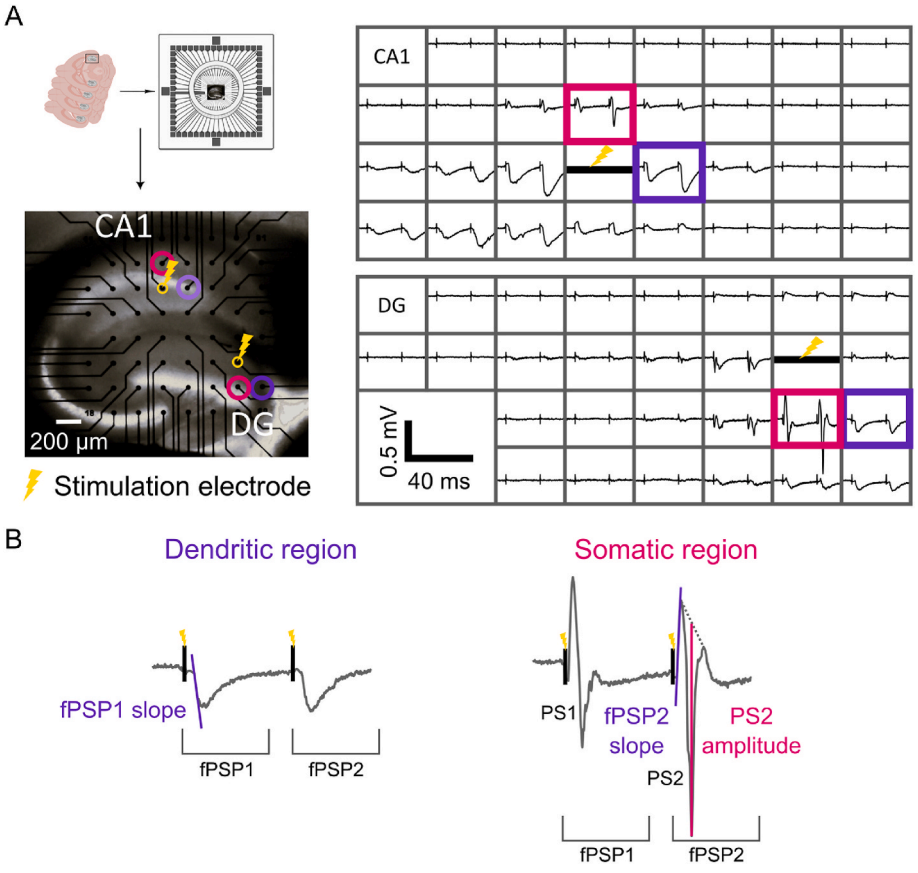


Fig. 1. Representative hippocampal MEA recording and signal parameters. A. Experimental setup showing a horizontal hippocampal slice positioned on the MEA, with the DG and CA1 regions aligned over the electrode grid (left). Representative fPSPs recorded across the DG and CA1 channels are shown (right). The stimulation electrode is indicated by a yellow lightning bolt symbol. The recording electrodes with the largest dendritic (purple) and somatic (pink) response are highlighted for both DG and CA1. B. Representative waveforms and measured parameters for the selected channels of DG. The dendritic signal (left) highlights the fPSP1 slope, while the somatic signal (right) highlights the fPSP2 slope and PS2 amplitude. Slopes are calculated via least-squares linear regression on the maximal falling (dendritic) or rising (somatic) phases of the fPSPs. The PS2 amplitude is measured as the vertical distance between its negative peak and the straight line connecting the positive peaks before and after the PS2. (For interpretation of the references to colour in this figure legend, the reader is referred to the Web version of this article.)

with a MEA1060 BC high-bandwidth pre-amplifier and digitized at 25 kHz with 16-bit resolution using MC_Rack software (Version 4.6.2, MCS, Reutlingen, Germany). Stimulation parameters (duration, amplitude, and repetition rate) were controlled via a programmable stimulator (STG4002; MCS, Reutlingen, Germany).

After the equilibration period, slice quality was tested by applying a monophasic negative voltage pulse (−2000 mV, duration 100 μs) consecutively to each electrode located in the DG stratum moleculare to stimulate the perforant path (PP) or in the CA1 stratum radiatum to stimulate the Schaffer collaterals (SCs), which resulted in dendritic and somatic fPSPs depending on the region of registration as described previously (Fig. 1A) (Vergaelen et al., 2024). In summary, upon stimulation of the DG input (*i.e.* PP fibers) or the CA1 input (*i.e.* the SCs) excitatory neurotransmission arises, causing a negative fPSP in the dendritic areas and a positive fPSP in somatic areas. At higher stimulation intensities, action potentials are generated in the granule cells (GCs) or pyramidal cells of the DG or CA1, respectively, causing a superposing negative potential, called a population spike (PS), in somatic areas (Strange et al., 2014; Johnston and Wu, 1995). Based on the shape of the fPSP, inferences can be made about neurotransmission, postsynaptic activation and neuronal excitability (Fig. 1B). The maximal slope of the negative of positive fPSP is a measure for the strength of neurotransmission (the input), whereas the PS amplitude is a measure for postsynaptic activation (the output). The ratio of PS amplitude to fPSP slope provides a proxy for excitability (Gorter et al., 2016). The use of a MEA allowed us to select the two optimal stimulation channels (one for DG and one for CA1) that yielded the largest and clearest responses, and to select the optimal registration electrodes for data-analysis for both regions (Hsiao et al., 2015). This is explained further in section 2.7 **Data-analysis**.

For all subsequent recordings, paired-pulse stimulation was performed using monophasic negative voltage pulses (100 μs duration, 20 ms interpulse interval). Responses to the first and second pulses were defined as fPSP1 and PS1, and fPSP2 and PS2, respectively. To determine the appropriate stimulation intensity for the following experimental paradigms, three input-output (I/O) curves were measured, consisting of paired pulses of increasing intensity (from −500 to −3500 mV in −250 mV increments) applied every 10 s. Depending on the specific protocol, a specific stimulation intensity was selected based on these I/O curves. The maximal stimulation intensity (I_{100}) was defined as the intensity where the dendritic or somatic response first saturated, or the maximum tested intensity if saturation did not occur. The half-maximal stimulation intensity (I_{50}) was calculated as the midpoint between the intensity associated with the first visible response and I_{100}.

2.6. Experimental protocols

2.6.1. Effect of the adenosine A_1 receptor agonist CPA on hippocampal evoked potentials

In a first series of experiments (**2.6.1 A**) the effect of different CPA concentrations on the slope of evoked fPSPs in DG and CA1 was evaluated in 3.25 K^+ aCSF. Multiple hippocampal slices were prepared from each animal (30 IHKA and 20 saline-injected control mice) and positioned on the MEA to record from either the DG or CA1, with the goal of obtaining data for both regions from each mouse. Following I/O curve recording and determination of the I_{50} for the dendritic fPSP1 slope, paired-pulse stimuli were delivered every 10 s for 90 min: 15 min baseline, 45 min CPA superfusion (10, 40, 100 or 900 nM; one concentration per slice) and 30 min wash-out.

In 3.25 mM K^+ aCSF, only 1 out of 25 slices of control mice showed a PS2 in the DG compared to 19 out of 27 slices from IHKA mice. To allow comparison of CPA effects on postsynaptic activation and excitability in slices from IHKA versus control mice, and additional experiment was performed with an adjusted protocol (**2.6.1 B**): the potassium concentration was increased up to 5.50 mM, in order to shift the potassium reversal potential and depolarize the resting membrane potential, and I/O curves were obtained with a maximal stimulation intensity of 5000 mV (instead of recording at the I_{50} stimulation intensity) (Somjen, 2002). In physiological cerebrospinal fluid (CSF), the extracellular potassium concentration is tightly regulated between 2.7 and 3.5 mM and even minor fluctuations can influence synaptic transmission (Somjen, 2002). Increasing K^+ concentration to 5.5 mM shifts the potassium reversal potential by approximately 14 mV according to the Nernst equation (Hammond, 2024). This depolarizing shift brings the resting state membrane potential closer to action potential threshold and enhances network excitability without inducing spontaneous epileptiform bursting, which typically requires extracellular potassium concentrations of $\geq$ 6.5 mM (Somjen, 2002; Raimondo et al., 2015; González et al., 2024). Slices from 14 IHKA mice and 7 saline-injected controls were positioned to cover both the DG and CA1 and alternating stimulation was applied between the DG and CA1 every 10 s to be able to record from both regions in the same slice. Only slices in which a PS could be evoked by the initial test pulses were selected for the recording protocol. This I/O protocol was repeated 12 times (76 min total): six repetitions during baseline (38 min) and six during superfusion with 40 nM CPA (38 min), which is in the range of its EC_{50} (Craey et al., 2026).

2.6.2. Subregion-selective suppression of dentate gyrus neurotransmission

To evaluate whether focal uncaging of CPA also has focal effects, patterned illumination was applied to the DG or CA1 in slices from 6 IHKA or 3 non-injected control mice, while MEA electrodes recorded fPSPs from both DG and CA1 and slices were superfused with 3 μM cCPA in 3.25 mM K^+ aCSF. No direct comparisons were carried out between slices from IHKA and healthy mice. Rather, the experiments in the non-injected control slices served as an initial feasibility test. Stimulation at I_{50} intensity was applied every 10 s, alternating between DG and CA1 for a total duration of 80 min. Following a 20-min baseline recording, ten flashes of a rectangular light pattern (658 × 486 μm, 100 ms flash duration, 4.7 mW/mm^2) was focused on the DG at 10 s interval. Forty minutes later (at min 60), an identical pattern of light flashes was focused on CA1 (Fig. 2). Illumination was controlled via a digital mirror device (Polygon 1000, Mightex, Canada) coupled to a high-power light-emitting diode (LED) (LCS-0405-65-22, Mightex, Canada). Light output was measured using a power meter with a photodiode sensor (S120VC coupled to PM100A, Thorlabs, Germany).

2.6.3. Closed-loop control of dentate gyrus postsynaptic activation

In a next experiment, we investigated whether closed-loop photopharmacology allowed to keep the PS2 amplitude, measured in DG of IHKA mice, close to a target level which is 50% lower compared to baseline. Hippocampal slices (n = 5) from IHKA mice were superfused with 3 μM cCPA in 3.25 mM K^+ aCSF and stimulated every 10s at I_{100} to evoke DG fPSPs.

The MEA channel with the largest PS2 amplitude was selected for real-time output via the audio channel of the MEA 1060 BC. This audio channel output was sampled using an external analog-to-digital (ADC) converter (NI-USB-6259, National Instruments, Austin, Tx, USA) and online-analysis of PS2 amplitude was performed using custom MATLAB-based software. The PS amplitude was calculated as the vertical distance between its negative peak and the straight line connecting the positive peaks before and after the PS (Fig. 1B).

Following a 15-min baseline recording, the 50% target threshold was calculated based on the average PS2 amplitude from the final 10 min of the baseline. During the subsequent 30-min closed-loop ON period, any recorded PS2 amplitude exceeding this target triggered a 25-ms, 405-nm light flash (0.06 mW/mm^2) to uncage cCPA. Recordings were concluded with a 15-min closed-loop OFF period.

2.7. Data-analysis

The offline analysis of fPSPs was performed using Matlab-based code (MATLAB R2024b, MathWorks, Natick, MA, USA). Two channels per

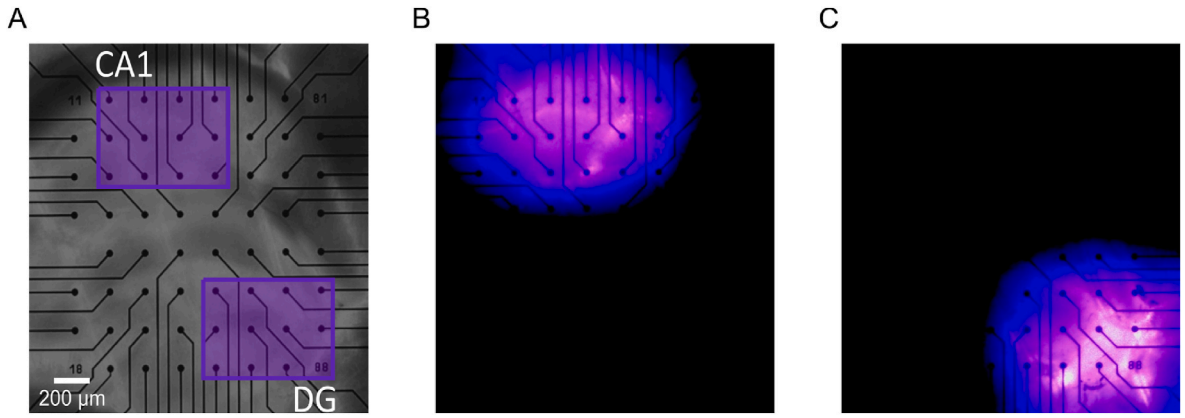


Fig. 2. Focal illumination of the DG and CA1. (A) Representative image of a hippocampal slice positioned on top of the MEA electrodes, illustrating the rectangular light pattern (658 × 486 µm) focused on the DG or CA1. (B-C) Images of the same hippocampal slice captured at the moment of illumination, showing the actual delivered light pattern targeting the CA1 (B) or DG (C) region.

region (DG and CA1) were selected based on: 1) largest negative dendritic fPSP in the stratum moleculare (DG) or the stratum radiatum (CA1) and 2) largest positive somatic fPSP with PS in the hilus (DG) or stratum oriens (CA1).

Specific parameters were selected for analysis based on their physiological meaning. fPSP1 slope of the dendritic fPSP was determined to evaluate changes in neurotransmission strength. Due to paired-pulse facilitation with the 20 ms inter-pulse interval, the PS2 was more robustly and frequently evoked than the PS1 (Gorter et al., 2016). Therefore, PS2 amplitude of the somatic fPSP was used to assess changes in postsynaptic activation. To evaluate changes in excitability, changes in the ratio of PS2 amplitude to the fPSP2 slope (i.e. the level of postsynaptic output for a given neurotransmission strength) were determined for the somatic fPSP. fPSP slopes were calculated via least-squares linear regression on the maximal falling (negative) or rising (positive) phases (Fig. 1B). PS2 amplitudes were calculated as explained higher. Only slices showing fPSP amplitudes larger than 100 µV at I_{50}, free of stimulation artefacts and with a stable baseline recording during the last 10 min (fluctuating within 95–105% of the baseline average) were included. For the experiments assessing CPA-mediated changes in excitability in 5.5 mM K^+ aCSF (**2.6.1 B**) and the closed-loop control of DG excitability (**2.6.3**), an additional inclusion criterion was used, namely PS2 amplitude had to be larger than 60 µV at I_{100}.

Statistical analysis and visualisations were conducted in R (R core team, Vienna, Austria), RStudio (Integrated Development for R, Boston, USA), GraphPad Prism (Version 10.6.1, Graphpad Software, Boston, USA) and the software Inkscape (version 1.4, www.inkscape.org). Linear mixed models were used for all comparisons unless stated otherwise, with the optimal random-effects structure (e.g. random intercepts for slices nested within animals and/or random slopes) selected via the Akaike information criterion (AIC). Slices from IHKA versus control mice is defined as "condition". A two-tailed p-value of < 0.05 with Bonferroni correction applied for multiple comparisons was used as significance cut-off. All values are reported as mean ± standard error of the mean (SEM) unless stated otherwise. Reported sample sizes (n) refer to the total number of slices, as the multilevel nature of the data was explicitly accounted for in the statistical models.

2.7.1. Effect of the adenosine A_1 receptor agonist CPA on hippocampal evoked potentials

To evaluate the effect of different CPA concentrations in 3.25 mM K^+ aCSF (**2.7.1 A**) in which fPSP recordings were performed at a fixed stimulation intensity (I_{50}), all data were normalized to the final 10 min of the baseline. For visualization, time-course data were plotted in 5-min bins. Statistical testing was performed using linear mixed models on the individual slice data during the final 10 min of the CPA superfusion period (t = 50-60), evaluating the main effect of CPA concentration and the CPA concentration × condition interaction. Because only one concentration was evaluated per slice, concentration-response curves were generated by fitting a non-linear regression model to the group means (±SEM). For both fPSP1 slope and PS2 amplitude, a fixed top of 100% (representing zero CPA effect) was used as well as a fixed Hill coefficient of −1. Population EC_{50} values and maximal effects were estimated and statistically compared between conditions with an extra sum-of-squares F-test.

For experiment **2.6.1 B**, we measured the area under the curve (AUC) of the fPSP1 slope and PS2 amplitude I/O curves and normalized them to the mean AUC of the last two baseline curves. For visualization, these normalized AUC values were plotted over time. The mean normalized AUC of the final two I/O curves during CPA superfusion was used for statistical comparison with a linear mixed model, evaluating the main effect of CPA concentration and the CPA concentration × condition interaction.

To evaluate changes in excitability, the fPSP2 slope and PS2 amplitude values were normalized to their respective maximum recorded during baseline. Linear regression was then performed for each individual slice for both baseline and CPA superfusion to extract the x-intercept and the regression slope. The x-intercept provides an estimate of the fPSP2 slope (i.e. neurotransmission strength) level needed to generate a PS2 (postsynaptic activation), while the regression slope represents the % increase of PS2 amplitude per % increase of fPSP2 slope. For visualization, mean regression lines were plotted using the group means for the x-intercept, regression slope and maximum fPSP2 slope. Linear mixed model analysis was used to evaluate the main effect of CPA concentration and CPA concentration × condition interaction.

The relative reduction in fPSP1 slope and PS2 amplitude induced by 40 nM CPA was compared between 3.25 mM K^+ and 5.5 mM K^+ conditions (**2.6.1 A versus B**) with a linear mixed model investigating the main effect of K^+ concentration per region or condition. For the 3.25 mM K^+ data, normalized values were averaged over the final 10 min of CPA superfusion. For the 5.5 mM K^+ data, the baseline I_{50} was determined for each slice, and the fPSP1 slope and PS2 amplitude values at this specific stimulation intensity were then extracted from the final two I/O curves during CPA superfusion and normalized to their corresponding baseline averages.

2.7.2. Subregion-selective suppression of dentate gyrus neurotransmission

To evaluate changes in fPSP1 slope after focal illumination of DG and CA1, data were normalized to the final 10 min of baseline and plotted as a continuous time course per recorded datapoint. For statistical analysis and visualization of the mean effect, data were re-normalized to the 10 min immediately preceding either DG or CA1 illumination. This was

implemented to account for any residual carryover effects following the first illumination period. The illumination effect window was defined as the 10-min period immediately following the first illumination pulse. Statistical evaluation was performed using a linear mixed model to analyse the main effect of illumination as well as the three-way interaction of illumination × illuminated region × recorded region. Post-hoc comparisons were subsequently applied to assess the impact of illumination within each recorded region independently.

2.7.3. Closed-loop control of dentate gyrus postsynaptic activation

For the closed-loop experiment, data were normalized to the final 10 min of the baseline. For visualization, these data were plotted in 5 min bins. Statistical analysis was performed on the quasi-steady-state averages evaluating the main effect of closed-loop illumination. The onset of the quasi-steady-state during the closed-loop ON period was defined as the time point at which the target (50% of baseline) was first reached following protocol initiation. The end of the quasi-steady-state was defined as the moment the closed-loop OFF period started. In addition to quasi-steady-state averages, the following parameters were quantified: (i) the duration of the time-to-target period (from the start of the closed-loop protocol to the onset of the quasi steady state), (ii) the average error to target during the quasi steady state, and (iii) the mean light flash interval between successive light flashes during the quasi steady state. Furthermore, we used a linear mixed model to compare PS2 amplitude to fPSP2 slope ratio's during the initial I/O curve, baseline and quasi steady state recordings to evaluate whether closed-loop suppression of PS2 amplitude was accompanied by shifts in neuronal excitability.

3. Results

3.1. Effect of the adenosine A_1 receptor agonist CPA on hippocampal evoked potentials

3.1.1. Concentration-dependent CPA-mediated suppression of field postsynaptic potentials

Representative fPSPs in Fig. 3A illustrate the inhibitory effect of the highest investigated CPA concentration (900 nM) on both dendritic and somatic fPSPs in 3.25 mM K^+.

In both the DG and CA1, CPA administration resulted in a concentration-dependent decrease of the fPSP1 slope in both groups ($p < 0.001$ for effect of CPA concentration, DG $t(94) = -11.54$, CA1 $t(8.7) = -7.77$, linear mixed model, Fig. 3B). This effect was significantly lower in the DG for slices of IHKA versus control mice ($p = 0.003$, $t(94) = 3.05$, for CPA concentration × condition interaction, linear mixed model, Fig. 3B). The estimated EC_{50} values based on the non-linear regression model to the group means did not significantly differ between IHKA and control slices in DG or CA1. For the DG, the estimated EC_{50} was 23 nM (95% CI: 4–76 nM) for IHKA slices and 14 nM (95% CI: 6–31 nM) for control slices. For the CA1, the estimated EC_{50} was 26 nM (95% CI: 5–78 nM) for IHKA slices and 19 nM (95% CI: 5–57 nM) for control slices. Instead, pair-wise model comparisons revealed a significant lower maximal effect in IHKA versus control slices for the DG, confirming the differences found with the linear mixed model analysis ($p = 0.001$, $F(48) = 11.50$, extra sum-of-squares F-test).

The likelihood of evoking a PS differed between conditions at baseline. In the DG, a PS2 could be measured in 19 out of 27 slices from IHKA mice, compared to only 1 out of 25 slices from controls. In the CA1, a PS2 was equally present in both groups (IHKA: 8/15; control: 7/19). A concentration-dependent reduction of PS2 amplitude was demonstrated in the DG of IHKA slices ($p < 0.001$, $t(6.3) = -15.81$, for CPA effect, linear mixed model; Fig. 3C). The estimated EC_{50} was 7 nM (95% CI: 2–17 nM). In the CA1, a concentration-dependent reduction of PS2 amplitude was demonstrated in both conditions ($p < 0.001$, $t(6.3) = -15.8$ for CPA concentration effect, linear mixed model, Fig. 3C), with a reduced effect for 10 nM CPA in IHKA versus control slices ($p < 0.001$, $t(6.2) = 6.38$, for CPA × condition interaction, linear mixed model, Fig. 3C). Due to the limited sample size, no estimation of EC_{50} was performed. Detailed steady-state data are provided in Table S1.

3.1.2. CPA-mediated suppression of field postsynaptic potentials in elevated potassium concentrations

To compare effects of CPA on postsynaptic activation and excitability between IHKA and control slices, additional experiments were performed in 5.5 mM K^+ aCSF and I/O curves were obtained using a range of 500 to 5000 mV to increase the likelihood of evoking a PS2. No spontaneous epileptiform activity was observed.

Representative examples of the AUC analysis of I/O curves are shown in Fig. 4A for the DG from an IHKA slice. Overall, a significant decrease in both fPSP1 slope and PS2 amplitude was demonstrated during 40 nM CPA superfusion in the DG ($p < 0.001$, CPA effect, IHKA: $n = 11$, fPSP1 slope $t(10) = -9.14$, PS2 amplitude $t(9.82) = -7.88$; control: $n = 9$, fPSP1 slope $t(6.21) = -7.35$, PS2 amplitude $t(6.96) = -8.65$; linear mixed model) and CA1 ($p = 0.01$, CPA effect, IHKA: $n = 6$, fPSP1 slope $t(14) = -3.39$, PS2 amplitude $t(8.69) = -4.16$, control: $n = 10$, fPSP1 slope $t(14) = -6.22$, PS2 amplitude $t(7.30) = -5.59$; linear mixed model, Fig. 4B) for IHKA and control slices. No significant differences could be demonstrated between the IHKA and control slices.

A representative example of the excitability analysis for an epileptic DG slice is illustrated in Fig. 5A. In this example, superfusion with 40 nM CPA increased the x-intercept from 61% minimal baseline fPSP2 slope to 66%. Also, the regression slope reduced from 2.33 to 0.86 during superfusion with 40 nM CPA. In total, for both regions (DG/CA1) and conditions (IHKA/control slices), CPA significantly increased in the x-intercept ($p < 0.001$, DG: $t(300) = -8.38$, CA1 $t(159) = -13.76$, linear mixed model) and reduced the regression slope (DG: $p = 0.003$, $t(301) = 2.96$, CA1: $p = 0.018$, $t(161) = -1.97$, linear mixed model, Fig. 5B). The shift in x-intercept was significantly smaller in IHKA compared to control slices for the CA1 ($p < 0.001$, $t(159) = -13.76$, linear mixed model).

We could not demonstrate statistically significant differences between the inhibitory effect of superfusing 40 nM CPA on fPSP1 slope evoked at I_{50} between 3.25 and 5.5 mM K^+ aCSF for both regions and conditions (Fig. 6A). However, a trend ($p = 0.097$, $t(16.6) = -1.76$, linear mixed model) towards more pronounced CPA effect on fPSP1 slope was noted in DG of control slices for 3.25 mM compared to 5.5 mM K+ aCSF. Due to the low incidence of PS in 3.25 mM K^+ aCSF conditions, statistical comparison for PS2 was not performed for the CA1 (IHKA or control slices) or DG control slices. For the DG in IHKA slices, CPA-induced suppression of PS2 amplitude was not significantly different between both K^+ concentrations ($p = 0.538$, $W = 24.5$, $n = 13$, Wilcoxon rank test, Fig. 6B).

3.2. Subregion-selective suppression of dentate gyrus neurotransmission

As illustrated in a representative example of a hippocampal slice from an IHKA mice which is continuously superfused with 3 μM cCPA, flashes of a rectangular light pattern that is focused on DG, suppresses fPSP in DG but has only limited effects on CA1 fPSP (Fig. 7A). If the light pattern is focused on CA1 the opposite is found; i.e. a pronounced fPSP inhibition in CA1 but not in DG (Fig. 7B).

Overall, both in IHKA ($n = 6$) and control ($n = 3$) slices, focal illumination produced a significant decrease in the fPSP1 slope specifically within the targeted hippocampal subregion (IHKA: $p = 0.001$, $t(35) = -3.59$; control: $p < 0.001$, $t(14) = 4.94$; for Illumination × Illuminated Region × Recorded Region interaction, linear mixed model; Fig. 7D). In contrast, no statistical significant effect could be demonstrated in the non-illuminated subregion (IHKA | DG as non-illuminated region: $t(35) = -0.32$, $p = 0.750$, CA1 as non-illuminated region: $t(35) = 0.62$, $p = 0.54$; control | DG as non-illuminated region: $t(14) = -0.56$, $p = 0.586$, CA1 as non-illuminated region: $t(14) = 1.19$, $p = 0.255$; linear mixed model).

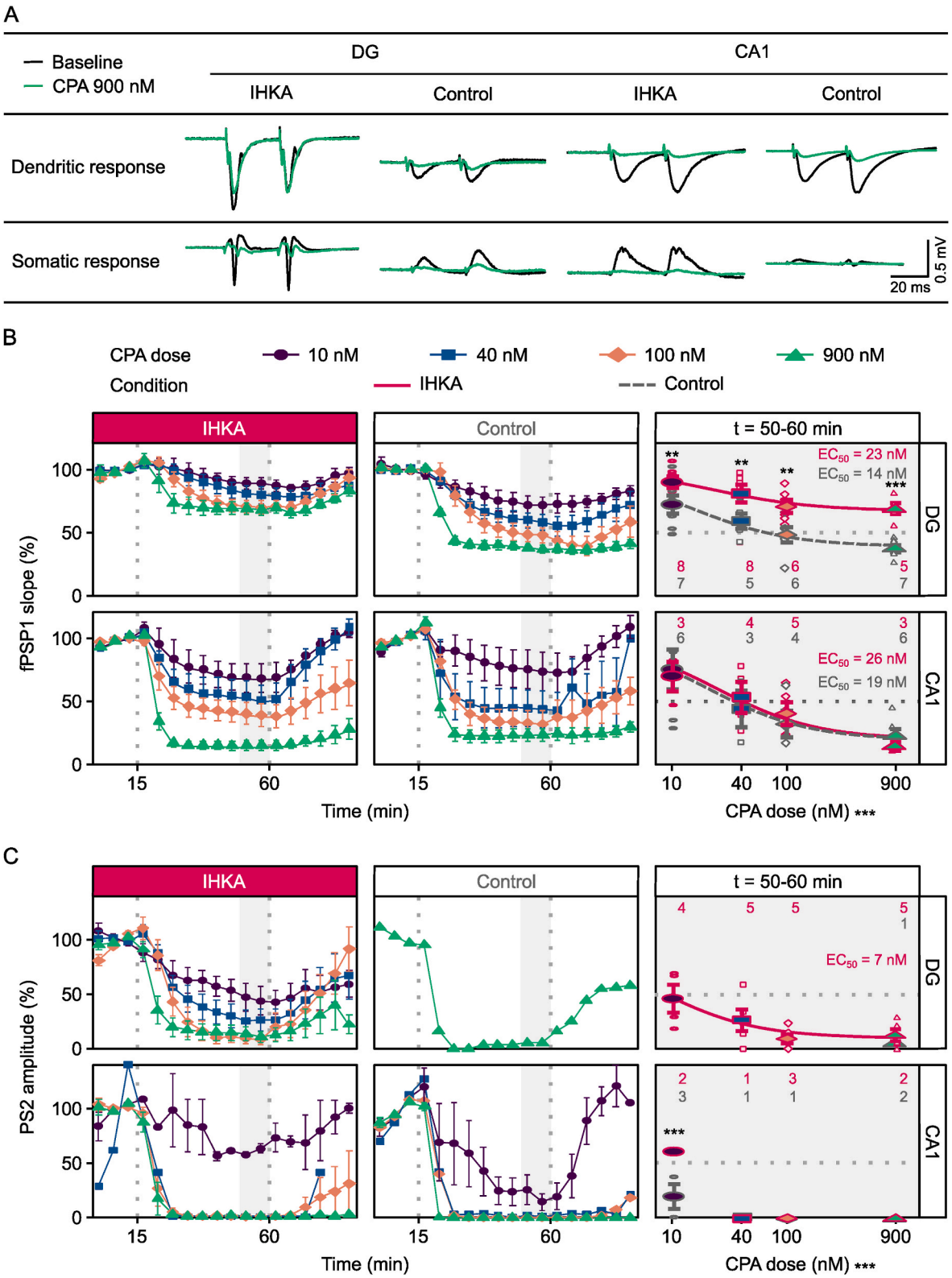


Fig. 3. CPA concentration-dependent suppression of neurotransmission strength and postsynaptic activation in DG and CA1 of hippocampal slices from IHKA versus control mice in 3.25 mM K^+ aCSF. (A) Representative examples of dendritic and somatic evoked fPSPs. Baseline traces are depicted in black; traces during CPA steady state (900 nM) are shown in green. (B-C) Concentration-dependent effect of CPA on fPSP1 slope (B) and PS2 amplitude (C) in DG and CA1 of slices from IHKA and control mice. Left and middle panels show the normalized effect over time (15 min baseline, 45 min CPA superfusion, 30 min washout). Vertical dashed lines indicate the start and end of CPA superfusion. The last 10 min used for analysis is highlighted with a grey background. Right panels show the concentration-response relationships of CPA. Sigmoidal curves are fitted to the group means ± SEM to estimate the EC_{50} values. The number of slices is indicated above or below each data point, and a grey dotted line serves as a reference for a 50% reduction level. Data are shown as mean ± SEM. **$p < 0.01$; ***$p < 0.001$. (For interpretation of the references to colour in this figure legend, the reader is referred to the Web version of this article.)

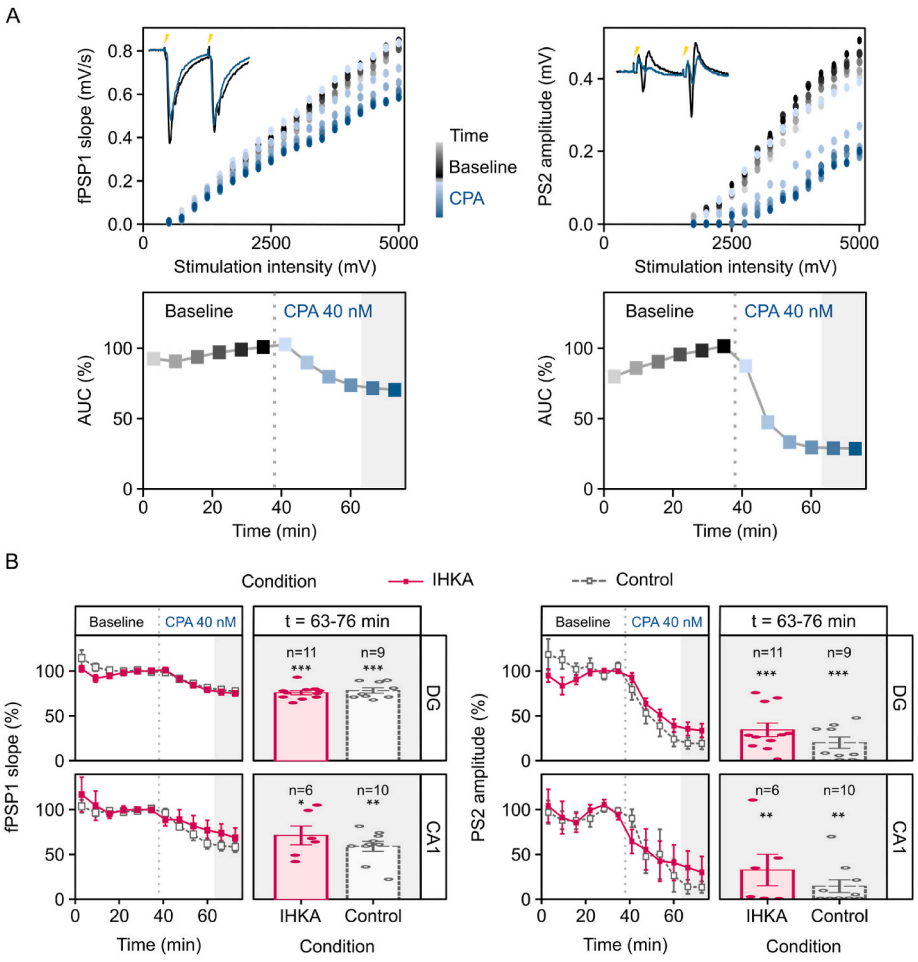


Fig. 4. CPA suppression of field postsynaptic potentials in DG and CA1 in slices from IHKA and control mice in 5.50 mM K^+ aCSF. (A) Representative AUC analysis for fPSP1 slope (left) and PS2 amplitude (right) in an epileptic DG slice. Top panels: 12 individual I/O curves; grey scaling indicates baseline curves; blue scaling indicates curves during CPA superfusion. Bottom panels: normalized AUC values plotted over time. The grey dotted vertical line indicates the switch to CPA superfusion. (B) Summary of normalized AUC values for fPSP1 slope (left) and PS2 amplitude (right) over time and at steady state (average of the last two I/O curves). Data are shown as mean ± SEM. *p < 0.05; **p < 0.01; ***p < 0.001. (For interpretation of the references to colour in this figure legend, the reader is referred to the Web version of this article.)

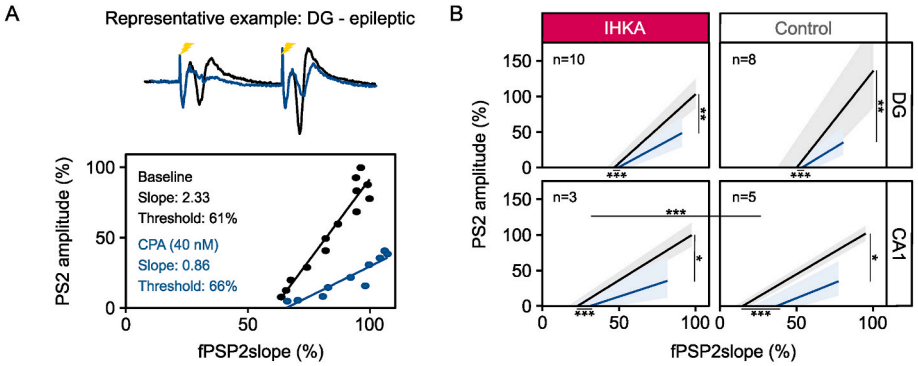


Fig. 5. CPA-dependent decrease in excitability (A) Representative excitability plot for the DG from an IHKA slice, showing the relationship between PS2 amplitude and fPSP2 slope during baseline (grey) and CPA steady state (blue). Lines represent linear regressions used to estimate PS2 threshold and gain. (B) Summary of the linear regression analysis for DG and CA1 in both IHKA and control slices. The plots show the normalized shift in the PS2 amplitude-to-fPSP2 slope relationship during 40 nM CPA superfusion (blue) compared to baseline (black). Data are shown as mean ± SEM. *p < 0.05; **p < 0.01; ***p < 0.001. (For interpretation of the references to colour in this figure legend, the reader is referred to the Web version of this article.)

Specifically, when the DG is illuminated, the DG fPSP1 slope decreased significantly to 67.7 ± 7.1% and 64.8 ± 9.9% of their baseline level in control and IHKA slices, respectively, while the CA1 fPSP1 slope slightly decreased, not reaching statistical significance, to 94.4 ± 2.1% and 95.3 ± 2.9% (Fig. 7D). Conversely, during CA1 illumination, the CA1 fPSP1 slope decreased significantly to 57.5 ± 7.2% and 73.1 ± 10.8%, while DG fPSP1 slope remained at baseline levels (i.e. 102.6 ± 3.9% and 102.4 ± 3.7%) in IHKA and control slices,

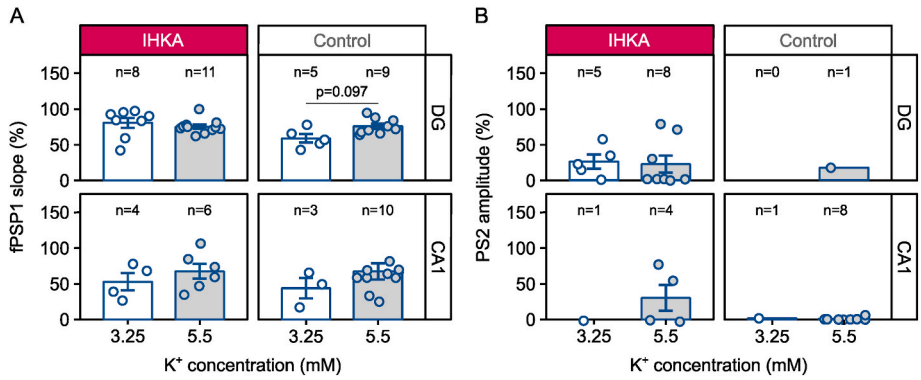


Fig. 6. Similar effect of 40 nM CPA on neurotransmission in slices superfused with 3.25 versus 5.50 mM K^+ aCSF. (A) fPSP1 slope and (B) PS2 amplitude during 40 nM CPA superfusion, expressed as a percentage of baseline at I_{50} stimulation intensity. Results are compared between slices superfused with 3.25 mM and 5.50 mM K^+ aCSF for both CA1 and DG in IHKA and control slices. Data are shown as mean ± SEM.

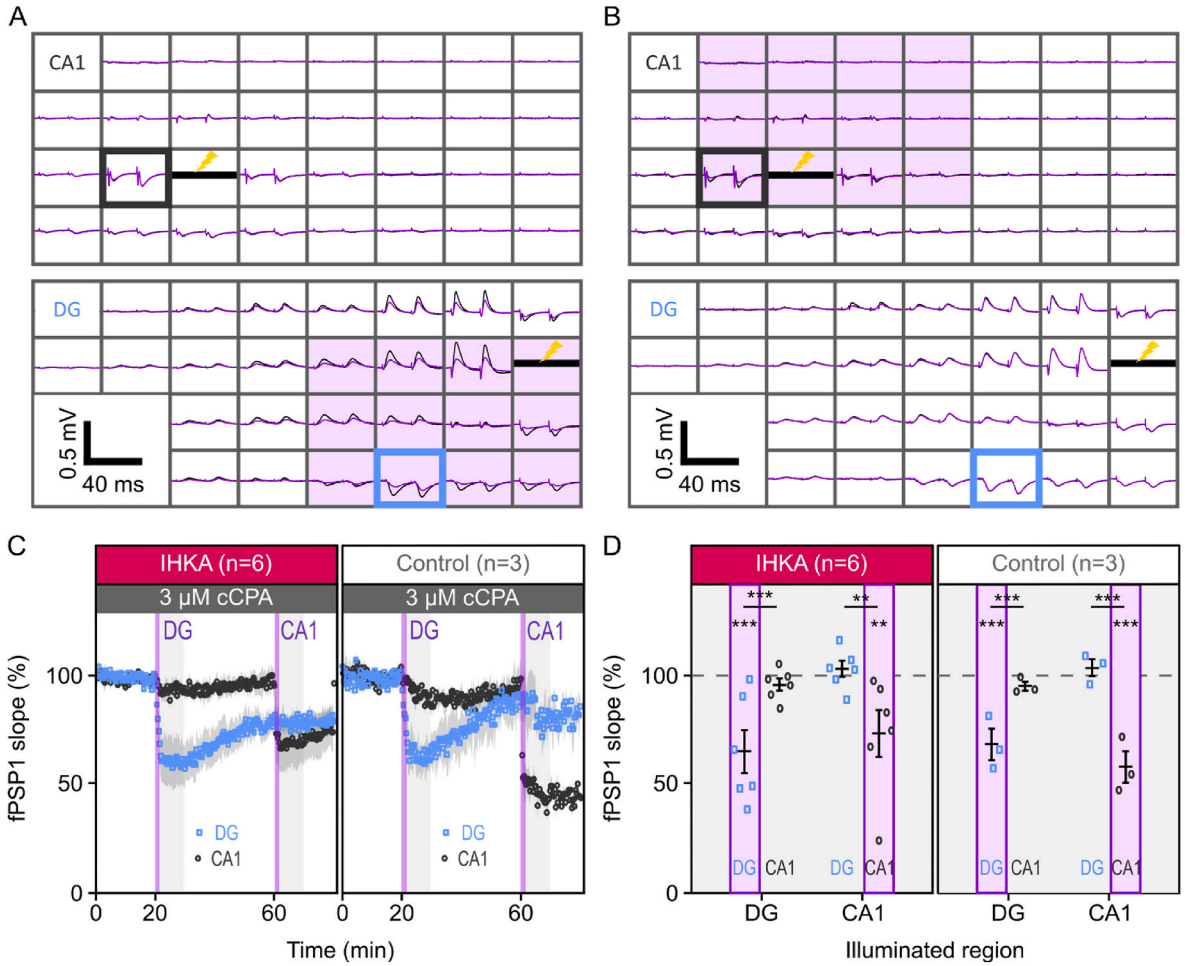


Fig. 7. Subregion-selective suppression of neurotransmission by cCPA and focal illumination. (A-B) Representative example of an IHKA slice illustrating the fPSP traces for DG (A) and CA1 (B) illumination. The stimulation electrode position is indicated by the lightning symbol. The analysed recording electrode in the dendritic region is depicted by blue (DG) and black (CA1) rectangle. Baseline traces are shown in black; traces following focal illumination are shown in purple. (C) Normalized fPSP1 slope (relative to the last 10 min of baseline) over time in IHKA (left) and control (right) slices incubated with 3 μM cCPA. Synaptic responses were recorded every 10 s, alternating in the DG (blue squares) or CA1 (black circles). The DG was illuminated at t = 20 min and the CA1 at t = 60 min, as indicated by the purple vertical bands (405 nm light, 10 pulses of 100 ms, 0.1 Hz, 0.3 mm^2, 4.7 mW/mm^2). The 10 min periods analysed starting from illumination are highlighted in grey. (D) Mean fPSP1 slope during the 10 min analysis window (expressed as a percentage of the 10 min pre-illumination baseline) for the DG (blue) and CA1 (black). The specific region targeted by focal illumination is highlighted by a purple colour. Data are presented as mean ± SEM. **p < 0.01; ***p < 0.001. (For interpretation of the references to colour in this figure legend, the reader is referred to the Web version of this article.)

respectively.

3.3. Closed-loop control of dentate gyrus postsynaptic activation

The final experiment evaluated the efficacy of a closed-loop photopharmacological approach to reduce and maintain PS2 amplitude in DG of IHKA slices (n = 5) at or below 50% of its baseline amplitude. Every 10 s an fPSP was evoked with I_{100} stimulation in IHKA slices superfused with 3 μM cCPA. An online algorithm analysed PS2 amplitude and each time it surmounted 50% of its baseline level a 25 ms flash of light was delivered to the slice.

A representative example of this experiment is illustrated in Fig. 8A. Following a 15 min baseline fPSP recording, the closed-loop protocol was activated resulting in a progressive decrease of PS2 amplitude reaching the 50% target level after 6.5 min. During the subsequent quasi-steady-state period, the closed-loop system maintained the PS2 amplitude around the 50% target level with a mean error of 3.6% by delivering light pulses every 27 s on average. During the closed-loop OFF period the PS2 amplitude gradually increased back towards baseline levels.

This feedback-triggered approach successfully maintained the PS2 amplitude near the 50% target level in all tested slices (Fig. 8B). Upon activation of the closed-loop, the mean time-to-target was 6.3 ± 1.2 min. During the quasi-steady-state period, the system operated with a mean interval between light pulses of 38.6 ± 5.6 s and a mean error to target of 5.5 ± 1.2%. During the quasi-steady-state period, the PS2 amplitude was significantly reduced to 45.7 ± 1.6% of baseline ($p < 0.001$, $t(5.66) = -38.95$, linear mixed model). This light-triggered CPA release was also associated with a significant reduction in the fPSP1 slope (93.1 ± 2.1% of baseline; $p < 0.001$, $F(1,8) = 80.58$, linear mixed model). Notably, the magnitude of suppression achieved via closed-loop CPA photorelease was comparable to the inhibitory effects observed following the superfusion of IHKA DG slices with 10 nM CPA under 3.25 mM K^+ conditions.

Finally, this closed-loop reduction of PS2 amplitude was associated with a reduction in neuronal excitability. The level of postsynaptic activation (PS2 amplitude) for a specific fPSP2 slope was already significantly lower during the baseline recording compared to the initial I/O curve ($p < 0.001$, $t(50.64) = 4.53$), linear mixed model). Crucially, the closed-loop steady state induced a further reduction in excitability, with the PS2 amplitude dropping an additional 32.8 ± 6.9% lower than during baseline recording ($p < 0.001$, $t(50.02) = 4.73$, linear mixed model, Fig. 8C).

4. Discussion

In this *ex vivo* study we addressed fundamental questions regarding the application of a closed-loop photopharmacological approach targeting the adenosine A_1R pathway within the epileptic DG. First, we demonstrated that adenosine A_1R activation using the agonist CPA remains an effective way of suppressing DG hyperexcitability in hippocampal slices from IHKA mice compared to controls. Furthermore, we showed subregion-selective suppression of neurotransmission strength in hippocampal slices superfused with our photocaged adenosine A_1R

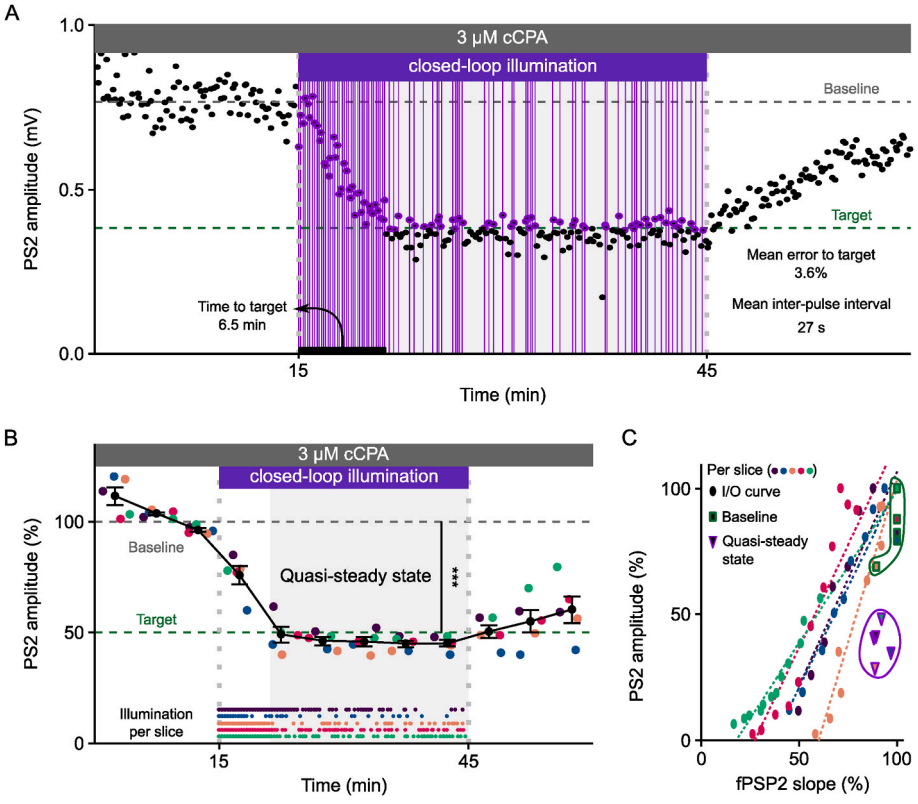


Fig. 8. Closed-loop photopharmacology maintains the DG PS2 amplitude at a predefined target level in IHKA slices. (A) Representative example of the PS2 amplitude over the time in a single IHKA slice. Between t = 15 and 45 min, the closed-loop system was activated. Whenever the PS2 amplitude exceeded the target threshold (50% of baseline, indicated by a purple outline around the datapoint), a light pulse (405 nm, vertical purple line) was automatically triggered. The initiation phase is highlighted by a black bar, the steady state by a grey background. (B) Mean normalized PS2 amplitude over time, shown as black dots. Individual PS2 amplitudes and the corresponding triggered illumination pulses for each slice are indicated by coloured markers. The average steady-state period is highlighted by a grey background. (C) Relationship between PS2 amplitude and fPSP2 slope. Data points are shown for each individual slice (in their respective colour) during the initial I/O curve recording (no outline), the pre-experimental baseline (green outline), and the closed-loop steady state (purple outline). Dashed lines represent the slice-specific linear regression fitted to the initial I/O curve data points representing the initial excitability. The five datapoints enclosed by the green or pink line, indicate the responses during the baseline and steady state, respectively. Data are shown as mean ± SEM. ***p < 0.001. (For interpretation of the references to colour in this figure legend, the reader is referred to the Web version of this article.)

agonist cCPA when subjected to focused illumination directed at either the DG or CA1. Finally, in slices from IHKA mice, a closed-loop photopharmacology algorithm was implemented, capable of recording DG population spikes as marker of postsynaptic activation and maintaining its amplitude at a stable level. Together, these findings demonstrate that the adenosine A_1R is a viable functional target for the precise, closed-loop control of DG hyperexcitability.

Our results confirm that adenosine A_1R-mediated inhibition remains functional in the epileptic hippocampus. A CPA concentration-dependent reduction of neurotransmission strength (fPSP1 slope) was found in DG and CA1 of IHKA and control slices in both 3.25 and 5.5 mM K^+ aCSF. Similarly, a CPA concentration-dependent reduction of postsynaptic activation (PS2 amplitude) was demonstrated in the DG of IHKA slices and the CA1 of IHKA and control slices in 3.25 mM K^+ aCSF and in both the DG and CA1 of IHKA and control slices in 5.5 mM K^+ aCSF. The CPA effect could not be evaluated for the DG of control slices in 3.25 mM K^+ aCSF, as PS occurrence was almost absent in the non-epileptic DG under physiological potassium concentration. This functional preservation of adenosine A_1R-mediated inhibition is further supported by our excitability analysis. Adenosine A_1R activation effectively increased the fPSP2 slope (i.e. neurotransmission strength) level needed to generate a PS2 and reduced postsynaptic activation/neurotransmission strength ratios in both hippocampal regions in control as well as IHKA slices (aside from a smaller threshold shift in the epileptic CA1) in 5.5 mM K^+ aCSF. The overall robust suppression of excitability within the epileptic hippocampus reinforces the adenosine A_1R as a valid and powerful target for precision seizure control. This is further supported by studies that could suppress epileptiform activity with adenosine A_1R activation in both *ex vivo* and *in vivo* models. Longo et al. (1995) observed CPA-mediated suppression of 4-aminopyridine (4-AP)-induced bursts in the CA1 of hippocampal slices, while Cano-Martınez et al. (2001) showed that pretreatment with CPA decreased KA-induced SE (Longo et al., 1995; Cano-Martınez et al., 2001). Furthermore, Gouder et al. (2003) could suppress seizures in the IHKA mouse model using an adenosine A_1R agonist which was further supported by our previous study using cCPA and DG illumination to suppress fPSPs in healthy mice and suppress seizures in IHKA mice *in vivo* (Gouder et al., 2003; Spanoghe et al., 2025).

Importantly, this study provides the first direct comparison of adenosine A_1R efficacy in hippocampal slices from IHKA versus control mice. While adenosine A_1R efficacy on neurotransmission strength was attenuated in the epileptic DG under physiological potassium concentrations (3.25 mM K^+), this difference disappeared under elevated potassium concentrations (5.5 mM K^+). This convergence was driven by a trend towards a reduction in the inhibitory response in the control slices in increased [K^+] conditions. In contrast, these differences between IHKA and non-epileptic control conditions could not be observed in the CA1.

These findings suggest that the reduced efficacy of adenosine A_1R signalling in the epileptic DG in physiological potassium conditions may be linked to the altered ionic environment and channel remodelling of the epileptic brain. Because the primary downstream mediator of the adenosine A_1R is the GIRK channel, its hyperpolarizing capacity depends directly on the extracellular potassium concentration and the resulting potassium equilibrium potential (E_K) (Somjen, 2002; Florence et al., 2012). Crucially, the functional impact of altering the potassium driving force is determined by how close a neuron's baseline resting membrane potential (V_{rest}) sits to the E_K. This differs between subfields and conditions. In the CA1, widespread expression of hyperpolarization-activated cyclic nucleotide-gated (HCN) channels drives a steady influx of Na^+ and K^+, maintaining a relatively depolarized V_{rest} around −65 mV (Malik et al., 2016; Bender et al., 2003; Biel et al., 2009; Kowalski et al., 2016). Conversely, granule cells in the healthy DG have a more hyperpolarized V_{rest} of −75 mV, more closely to the E_K. This hyperpolarized state is sustained not only by low HCN channel expression but also by a higher density of background potassium leak channels, and therefore depends heavily on the extracellular potassium concentration (Kowalski et al., 2016). Under epileptic conditions, however, spatial potassium buffering by astrocytes is decreased resulting in localized accumulation of K^+ and HCN channels are more widely expressed, which could decrease the hyperpolarizing potential of GIRK channels. These differences between healthy and epileptic DG could be masked when the overall extracellular potassium concentration is increased. Moreover, the increased extracellular potassium concentration affects the healthy granule cells the most, as these cells are most depending on E_K (Häussler et al., 2012; Florence et al., 2012; Bender et al., 2003; Schmidt-Hieber et al., 2004; Kinboshi et al., 2020).

A previous study by Rebola et al. (2003) attributed observed differences in CPA-mediated fPSP suppression in the CA1 in hippocampal slices from epileptic kindled rats compared to healthy controls to a difference in receptor density and binding density (Rebola et al., 2003). Indeed, both increases and decreases in adenosine A_1R are being reported in animal models of epilepsy and resected tissue from epilepsy patients (Ekonomou et al., 2000; Rebola et al., 2003; Angelatou et al., 1993; Glass et al., 1996; Ådén et al., 2004; Tchekalarova et al., 2005; Hendricks et al., 2019). However, our functional data suggest that receptor density alone is not the primary determinant of therapeutic efficacy, further supported by a similar estimated EC_{50} for the concentration-response curves for the fPSP1 slope in both CA1 and DG. Even though the exact underlying mechanisms are not clear and not directly investigated in this study, our data suggests that the adenosine A_1R signalling pathway remains functionally intact but subject to environmental modulation. This supports the hypothesis that failure of endogenous adenosine as a seizure suppressant is more likely due to its chronic depletion via upregulated adenosine kinase than a fundamental loss of receptor signalling integrity (Weltha et al., 2019; Baltos et al., 2024).

An important limitation of this study is the exclusive use of male mice, given the potential sex differences in adenosine A_1R signalling. For example, although Pinto et al. (2016) found no clear sex differences in CPA-mediated effects on neurotransmission in hippocampal slices from healthy rats, differences emerged depending on which part of the downstream guanyl cyclase pathway was blocked (Pinto et al., 2016). Furthermore, Borgus et al. (2020) found that female rats have a higher basal adenosine concentration in the CA1 influenced by the oestrous cycle, whereas Pierling et al. (2021) observed higher adenosine A_1R availability throughout the brain in healthy female participants measured by positron emission tomography (PET) (Borgus et al., 2020; Pierling et al., 2021). Therefore, validating these adenosine A_1R efficacy results in female cohorts will be an important step for future studies.

Beyond characterizing the adenosine A_1R as a functional target, this study demonstrated the feasibility of subregion-selective suppression within the epileptic hippocampal circuit. By combining continuous superfusion of hippocampal slices with the photocaged adenosine A_1R agonist, cCPA, and patterned illumination under microscopic control, neuronal inhibition could be targeted to the DG while limiting the effects in the CA1 and vice versa. The *ex vivo* conditions might have contributed to achieving this spatial specificity. Continuous superfusion of CPA containing aCSF likely facilitated homogeneous wash-in of cCPA and accelerated wash-out of cCPA, thereby preventing CPA to reach bioactive concentrations in non-illuminated regions (Krook-Magnuson et al., 2015b; Scharfman, 2019). Furthermore, in hippocampal slices, DG and CA1 are less connected compared to intact brain conditions, which facilitates their independent modulation (Liu et al., 2012). It is important to emphasize that this degree of spatial targeting will likely be less pronounced *in vivo* due to the blood-brain barrier, and different tissue perfusion dynamics and intercircuit propagation of neuromodulatory effects. Nevertheless, subregion-specific targeting remains a compelling concept in mTLE-HS, where pathological changes primarily impair the dentate gate (Krook-Magnuson et al., 2015b; Scharfman, 2019). Constraining adenosine A_1R activation mainly to the DG could theoretically

minimize central side effects like sedation or memory impairment, though achieving such localized suppression in intact brain tissue, the efficacy and the impact on cognitive functioning remains to be investigated (Borea et al., 2018b). While our previous *in vivo* study observed seizure suppression and improved tolerability based on rotarod performance following cCPA uncaging in DG, the present work provides electrophysiological validation (Spanoghe et al., 2025).

While other focal adenosine-based therapies, such as silk-based adenosine implants, encapsulated cells or stem cell-derived brain implants have shown promise, photopharmacology offers the unique added value of temporal control (Boison and Stewart, 2009). Therefore, a photopharmacological closed-loop system capable of regulating DG postsynaptic output was investigated. Unlike closed-loop approaches that reactively terminate seizures once they started, our approach aims for an adaptive stabilization of DG excitability (Krook-Magnuson et al., 2015b; Ramgopal et al., 2014; Cherian and Kanaga, 2022; Gielen and Wadman, 2003). By sampling the PS2 amplitude at 0.1 Hz, analysing its parameters in quasi real-time and triggering light pulses when the value surmounted a threshold level, we could maintain the DG output at a stable reduced level. Given that granule cells in the epileptic DG are hyperexcitable, merely limiting neurotransmission strength (fPSP1 slope), may not prevent excessive postsynaptic output (Krook-Magnuson et al., 2015b; Häussler et al., 2012; Hendricks et al., 2019; Scharfman, 2019). By supressing the postsynaptic activation, we regulate the final output of the dentate gate regardless of the neurotransmission strength. This choice is further supported by the finding that the decrease in postsynaptic activation is associated with a decrease in excitability. This approach could allow us to maintain neuronal activity below the detection threshold while effectively preventing excessive output that could lead to seizures. Lepeu et al. (2024) showed in mice using optogenetically-evoked fPSPs that there is a critical tipping point in excitability during which fPSPs are largely increased and a seizure follows. Moreover, they were able to record electrically-evoked fPSPs in humans undergoing intracranial electroencephalography (iEEG) in the context of presurgical evaluation. These fPSPs decreased following Benzodiazepine administration, a known inhibitor of excitability (Lepeu et al., 2024). Similarly, Graham et al. (2023) showed *ex vivo* in hippocampal slices using Mg^{2+}-free aCSF and *in vivo* using 4-aminopyridine (4-AP) that acute seizures were preceded by a critical increase in fPSPs right before onset of seizure-like activity (Graham et al., 2023).

Although closed-loop photopharmacological modulation of the adenosine A_1R seems promising, its application potential in clinical practice remains to be investigated and requires addressing major translational hurdles. First, maintaining effective local concentrations of cCPA *in vivo* without diffusion of the uncaged compound into off-target brain regions presents a major pharmacokinetic challenge. Addressing this will require detailed pharmacodynamic and -kinetic studies incorporating multi-site microdialysis and electrophysiological monitoring, as well as the potential development of novel photocaged derivatives if cCPA proves suboptimal regarding safety (Ganzoni et al., 2025). Second, continuous recording evoked responses (such as DG population spikes) in freely moving, chronically epileptic animals is technically difficult. Future *in vivo* systems will need to identify robust electrophysiological proxies for excitability or seizure risk (Buzsáki, 2004; Boon et al., 2009). Finally, light delivery to deep brain structures like the hippocampus requires the development of safe, biocompatible light-emitting probes (Ganzoni et al., 2025). Resolving these intermediate challenges will be essential to evaluate whether the theoretical benefits of closed-loop photopharmacology can be realized in an epilepsy model *in vivo*.

In conclusion, this study confirmed that adenosine A_1R activation remains an effective and robust mechanism for reducing excitability in the epileptic IHKA hippocampus. By using a photocaged adenosine A_1R agonist, we demonstrated that this inhibition can be spatially targeted, providing a pathway to avoid systemic adenosine A_1R-mediated side effects. Finally, the success of our closed-loop photopharmacology approach which maintained the DG postsynaptic activation at a predefined target level, highlights the potential of photopharmacology to prevent episodes of hyperexcitability. Together, these findings reinforce photopharmacological adenosine A_1R activation as a promising targeted approach for pharmacoresistant mTLE-HS.

CRediT authorship contribution statement

Marijke Vergaelen: Conceptualization, Formal analysis, Investigation, Methodology, Validation, Visualization, Writing – original draft, Writing – review & editing. **Kristl Vonck:** Conceptualization, Formal analysis, Funding acquisition, Investigation, Methodology, Project administration, Resources, Supervision, Validation, Visualization, Writing – review & editing. **Ruben Tack:** Conceptualization, Writing – review & editing. **Melissa Lajtos:** Conceptualization, Writing – review & editing. **Simona Manzella:** Conceptualization, Formal analysis, Investigation, Methodology, Validation, Writing – review & editing. **Jeroen Missinne:** Conceptualization, Funding acquisition, Methodology, Project administration, Resources, Writing – review & editing. **Mathieu Sprengers:** Conceptualization, Methodology, Writing – review & editing. **Evelien Carrette:** Conceptualization, Funding acquisition, Methodology, Project administration, Writing – review & editing. **Paul Boon:** Conceptualization, Funding acquisition, Methodology, Project administration, Resources, Writing – review & editing. **Serge Van Calenbergh:** Conceptualization, Funding acquisition, Methodology, Project administration, Resources, Writing – review & editing. **Robrecht Raedt:** Conceptualization, Formal analysis, Funding acquisition, Investigation, Methodology, Project administration, Resources, Supervision, Validation, Visualization, Writing – review & editing.

Funding

This research was funded by the Ghent University Special Research Fund, This research was funded by the Ghent University Special Research Fund (grant number 01G02722), the Queen Elisabeth Medical Foundation, and Research Foundation Flanders-FWO (grant numbers G075224N and G027422N).

Declaration of competing interests

The authors report no competing interests.

Appendix A. Supplementary data

Supplementary data to this article can be found online at https://doi.org/10.1016/j.neuropharm.2026.111152.

References

Ådén, U., O'Connor, W.I., Berman, R.F., 2004. Changes in purine levels and adenosine receptors in kindled seizures in the rat. Neuroreport 15 (10), 1585–1589. https://doi.org/10.1097/01.WNR.0000133227.94662.C9.

Androsova, G., Krause, R., Borghei, M., Wassenaar, M., Auce, P., Avbersek, A., et al., 2017. Comparative effectiveness of antiepileptic drugs in patients with mesial temporal lobe epilepsy with hippocampal sclerosis. Epilepsia 58 (10), 1734–1741. https://doi.org/10.1111/epi.13871.

Angelatou, F., Pagonopoulou, O., Maraziotis, T., Olivier, A., Villemeure, J.G., Avoli, M., et al., 1993. Upregulation of A1 adenosine receptors in human temporal lobe epilepsy: a quantitative autoradiographic study. Neurosci. Lett. 163 (1), 11–14. https://doi.org/10.1016/0304-3940(93)90217-9.

Baltos, J.A., Casillas-Espinosa, P.M., Rollo, B., Gregory, K.J., White, P.J., Christopoulos, A., et al., 2024. The role of the adenosine system in epilepsy and its comorbidities. Br. J. Pharmacol. 181 (14), 2143–2157. https://doi.org/10.1111/bph.16094.

Bender, R.A., Soleymani, S.V., Brewster, A.L., Nguyen, S.T., Beck, H., Mathern, G.W., et al., 2003. Enhanced expression of a specific hyperpolarization-activated cyclic nucleotide-gated cation channel (HCN) in surviving dentate gyrus granule cells of human and experimental epileptic hippocampus. J. Neurosci. 23 (17), 6826–6836. https://doi.org/10.1523/JNEUROSCI.23-17-06826.2003.

Biel, M., Wahl-Schott, C., Michalakis, S., Zong, X., 2009. Hyperpolarization-activated cation channels: from genes to function. Physiol. Rev. 89 (3), 847–885. https://doi.org/10.1152/physrev.00029.2008.

Bjørke, A.B., Nome, C.G., Falk, R.S., Gjerstad, L., Taubøll, E., Heuser, K., 2018. Evaluation of long-term antiepileptic drug use in patients with temporal lobe epilepsy: assessment of risk factors for drug resistance and polypharmacy. Seizure 61, 63–70. https://doi.org/10.1016/j.seizure.2018.07.011.

Boison, D., Stewart, K.A., 2009. Therapeutic epilepsy research: from pharmacological rationale to focal adenosine augmentation. Biochem. Pharmacol. 78 (12), 1428–1437. https://doi.org/10.1016/j.bcp.2009.08.005.

Boon, P., Raedt, R., De Herdt, V., Wyckhuys, T., Vonck, K., 2009. Electrical stimulation for the treatment of epilepsy, 6, 218–227. https://doi.org/10.1016/j.nurt.2008.12.003.

Borea, P.A., Gessi, S., Merighi, S., Vincenzi, F., Varani, K., 2018b. Pharmacology of adenosine receptors: the state of the art. Physiol. Rev. 98 (3), 1591–1625. https://doi.org/10.1152/physrev.00049.2017.

Borea, P.A., Gessi, S., Vincenzi, F., Varani, K., Merighi, K. (Eds.), 2018a. The Adenosine Receptors, 34. Humana Press. https://doi.org/10.1007/978-3-319-90808-3.

Borgus, J.R., Puthongkham, P., Venton, B.J., 2020. Complex sex and estrous cycle differences in spontaneous transient adenosine. J. Neurochem. 153 (2), 216–229. https://doi.org/10.1111/jnc.14981.

Buzsáki, G., 2004. Large-scale recording of neuronal ensembles. Nat. Neurosci. 7 (5), 446–451. https://doi.org/10.1038/nn1233.

Cano-Martınez, A., Villalobos-Molina, R., Rocha, L., 2001. Effects of chronic morphine and *N*6-cyclopentyl-adenosine administration on kainic acid-induced status epilepticus. Epilepsy Res. 44 (2), 89–96. https://doi.org/10.1016/S0920-1211(01)00187-5.

Cherian, R., Kanaga, E.G., 2022. Theoretical and methodological analysis of EEG based seizure detection and prediction: an exhaustive review. J. Neurosci. Methods 369. https://doi.org/10.1016/j.jneumeth.2022.109483.

Craey, E., Hulpia, F., Spanoghe, J., Manzella, S., Larsen, L.E., Sprengers, M., et al., 2022. Ex vivo feedback control of neurotransmission using a photocaged adenosine A1 receptor agonist. Int. J. Mol. Sci. 23 (16). https://doi.org/10.3390/ijms23168887.

Craey, E., Vergaelen, M., Van Calenbergh, S., Spanoghe, J., Carrette, E., Vonck, K., et al., 2026. Feedback control of excitability and high K+ induced epileptiform bursts in male rat hippocampal slices with a photocaged adenosine A1 receptor agonist. Br. J. Pharmacol. https://doi.org/10.1111/bph.70349.

Desloovere, J., Boon, P., Lars, Larsen, E., Goossens, M.G., Delbeke, J., et al., 2021. Chemogenetic seizure control with clozapine and the novel ligand JHU37160 outperforms the effects of levetiracetam in the intrahippocampal kainic acid mouse model. Neurotherapeutics 19 (1), 342–351. https://doi.org/10.1007/S13311-021-01160-0, 2021 19:1.

Desloovere, J., Boon, P., Larsen, L.E., Merckx, C., Goossens, M., Van den Haute, C., et al., 2019. Long-term chemogenetic suppression of spontaneous seizures in a mouse model for temporal lobe epilepsy. Epilepsia 60 (11), 2314–2324. https://doi.org/10.1111/epi.16368.

Ekonomou, A., Sperk, G., Kostopoulos, G., Angelatou, F., 2000. Reduction of A1 adenosine receptors in rat hippocampus after kainic acid-induced limbic seizures. Neurosci. Lett. 284 (1–2), 49–52. https://doi.org/10.1016/S0304-3940(00)00954-X.

Florence, G., Pereira, T., Kurths, J., 2012. Extracellular potassium dynamics in the hyperexcitable state of the neuronal ictal activity. Commun. Nonlinear Sci. Numer. Simul. 17 (12), 4700–4706. https://doi.org/10.1016/j.cnsns.2011.06.023.

Ganzoni, R.L.Z., Bournons, S.S., Carreira, E.M., De Bundel, D., Smolders, I., 2025. A bright future for photopharmaceuticals addressing central nervous system disorders: state of the art and challenges toward clinical translation. Med. Res. Rev. 45 (5), 1323–1374. https://doi.org/10.1002/med.22105.

Gielen, F., Wadman, W., 2003. Closed loop neuromodulation for suppression of epileptic activity. U.S. Patent No. US-6671555-B2.

Glass, M., Faull, R.L.M., Bullock, J.Y., Jansen, K., Mee, E.W., Walker, E.B., et al., 1996. Loss of A1 adenosine receptors in human temporal lobe epilepsy. Brain Res. 710 (1–2), 56–68. https://doi.org/10.1016/0006-8993(95)01313-X.

González, O.C., Timofeev, I., Bazhenov, M., 2024. Role of ion concentration dynamics in epileptic seizures. In: Noebels, J.L., Avoli, M., Rogawski, M.A., Vezzani, A., Delgado-Escueta, A.V. (Eds.), Jasper's Basic Mechanisms of the Epilepsies, fifth ed. Oxford University Press, New York.

Gorter, J.A., van Vliet, E.A., Lopes da Silva, F.H., 2016. Which insights have we gained from the kindling and post-status epilepticus models? J. Neurosci. Methods 260, 96–108. https://doi.org/10.1016/J.JNEUMETH.2015.03.025.

Gouder, N., Fritschy, J.M., Boison, D., 2003. Seizure suppression by adenosine A1 receptor activation in a mouse model of pharmacoresistant epilepsy. Epilepsia 44 (7), 877–885. https://doi.org/10.1046/j.1528-1157.2003.03603.x.

Graham, R.T., Parrish, R.R., Alberio, L., Johnson, E.L., Owens, L., Trevelyan, A.J., 2023. Optogenetic stimulation reveals a latent tipping point in cortical networks during ictogenesis. Brain: J. Neurol. 146 (7), 2814–2827. https://doi.org/10.1093/brain/awac487.

Hammond, C., 2024. Cellullar and Molecular Neurophysiology. Academic Press, Fifth. https://doi.org/10.1016/C2020-0-03928-9.

Häussler, U., Bielefeld, L., Froriep, U.P., Wolfart, J., Haas, C.A., 2012. Septotemporal position in the hippocampal formation determines epileptic and neurogenic activity in temporal lobe epilepsy. Cerebr. Cortex 22 (1), 26–36. https://doi.org/10.1093/cercor/bhr054.

Hendricks, W.D., Westbrook, G.L., Schnell, E., 2019. Early detonation by sprouted mossy fibers enables aberrant dentate network activity, 13 (22), 10994–10999. https://doi.org/10.1073/pnas.1821227116.

Hsiao, M.C., Yu, P.N., Song, D., Liu, C.Y., Heck, C.N., Millett, D., et al., 2015. An in vitro seizure model from human hippocampal slices using multi-electrode arrays. J. Neurosci. Methods 244, 154–163. https://doi.org/10.1016/j.jneumeth.2014.09.010.

Johnston, D., Wu, SM sin, 1995. Foundations of Cellular Neurophysiology. MIT Press, p. 676.

Kalilani, L., Sun, X., Pelgrims, B., Noack-Rink, M., Villanueva, V., 2018. The epidemiology of drug-resistant epilepsy: a systematic review and meta-analysis. Epilepsia 59 (12), 2179–2193. https://doi.org/10.1111/epi.14596.

Kinboshi, M., Ikeda, A., Ohno, Y., 2020. Role of astrocytic inwardly rectifying potassium (Kir) 4.1 channels in epileptogenesis. Front. Neurol. 11. https://doi.org/10.3389/fneur.2020.626658.

Kowalski, J., Gan, J., Jonas, P., Pernía-Andrade, A.J., 2016. Intrinsic membrane properties determine hippocampal differential firing pattern in vivo in anesthetized rats. Hippocampus 26 (5), 668–682. https://doi.org/10.1002/hipo.22550.

Krook-Magnuson, E., Armstrong, C., Bui, A., Lew, S., Oijala, M., Soltesz, I., 2015b. In vivo evaluation of the dentate gate theory in epilepsy. J. Physiol. (Paris) 593 (10), 2379–2388. https://doi.org/10.1113/JP270056.

Krook-Magnuson, E., Gelinas, J.N., Soltesz, I., Buzsáki, G., 2015a. Neuroelectronics and biooptics: closed-loop technologies in neurological disorders. JAMA Neurol. 72 (7), 823–829. https://doi.org/10.1001/jamaneurol.2015.0608.

Krueppel, R., Remy, S., Beck, H., 2011. Dendritic integration in hippocampal dentate granule cells. Neuron 71 (3), 512–528. https://doi.org/10.1016/j.neuron.2011.05.043.

Le Duigou, C., Bouilleret, V., Miles, R., 2008. Epileptiform activities in slices of hippocampus from mice after intra-hippocampal injection of kainic acid. J. Physiol. (Paris) 586 (20), 4891–4904. https://doi.org/10.1113/jphysiol.2008.156281.

Le Duigou, C., Wittner, L., Danglot, L., Miles, R., 2005. Effects of focal injection of kainic acid into the mouse hippocampus in vitro and ex vivo. J. Physiol. (Paris) 569 (3), 833–847. https://doi.org/10.1113/jphysiol.2005.094599.

Lee, C.T., Kao, M.H., Hou, W.H., Wei, Y.T., Chen, C.L., Lien, C.C., 2016. Causal evidence for the role of specific GABAergic interneuron types in entorhinal recruitment of dentate granule cells. Sci. Rep. 6 (1), 36885. https://doi.org/10.1038/srep36885.

Lepeu, G., van Maren, E., Slabeva, K., Friedrichs-Maeder, C., Fuchs, M., Z'Graggen, W.J., et al., 2024. The critical dynamics of hippocampal seizures. Nat. Commun. 15 (1), 6945. https://doi.org/10.1038/s41467-024-50504-9.

Liu, M.G., Chen, X.F., He, T., Li, Z., Chen, J., 2012. Use of multi-electrode array recordings in studies of network synaptic plasticity in both time and space. Neurosci. Bull. 28 (4), 409. https://doi.org/10.1007/S12264-012-1251-5.

Liu, Y.C., Cheng, J.K., Lien, C.C., 2014. Rapid dynamic changes of dendritic inhibition in the dentate gyrus by presynaptic activity patterns. J. Neurosci. : the official journal of the Society for Neuroscience 34 (4), 1344–1357. https://doi.org/10.1523/JNEUROSCI.2566-13.2014.

Longo, R., Zeng, Y.C., Sagratella, S., 1995. Opposite modulation of 4-aminopyridine and hypoxic hyperexcitability by A1 and A2 adenosine receptor ligands in rat hippocampal slices. Neurosci. Lett. 200 (1), 21–24. https://doi.org/10.1016/0304-3940(95)12064-B.

Malik, R., Dougherty, K.A., Parikh, K., Byrne, C., Johnston, D., 2016. Mapping the electrophysiological and morphological properties of CA1 pyramidal neurons along the longitudinal hippocampal axis. Hippocampus 26 (3), 341–361. https://doi.org/10.1002/hipo.22526.

Pierling, A.L., Elmenhorst, E.M., Lange, D., Hennecke, E., Baur, D.M., Beer, S., et al., 2021. Cerebral A1 adenosine receptor availability in female and male participants and its relationship to sleep. Neuroimage 245, 118695. https://doi.org/10.1016/j.neuroimage.2021.118695.

Pinto, I., Serpa, A., Sebastião, A.M., Cascalheira, J.F., 2016. The role of cGMP on adenosine A1 receptor-mediated inhibition of synaptic transmission at the hippocampus. Front. Pharmacol. 7. https://doi.org/10.3389/fphar.2016.00103.

Raimondo, J.V., Burman, R.J., Katz, A.A., Akerman, C.J., 2015. Ion dynamics during seizures. Front. Cell. Neurosci. 9. https://doi.org/10.3389/fncel.2015.00419.

Ramgopal, S., Thome-Souza, S., Jackson, M., Kadish, N.E., Sánchez Fernández, I., Klehm, J., et al., 2014. Seizure detection, seizure prediction, and closed-loop warning systems in epilepsy. Epilepsy Behav. 37, 291–307. https://doi.org/10.1016/j.yebeh.2014.06.023.

Rebola, N., Coelho, J.E., Costenla, A.R., Lopes, L.V., Parada, A., Oliveira, C.R., et al., 2003. Decrease of adenosine A1 receptor density and of adenosine neuromodulation the hippocampus of kindled rats. Eur. J. Neurosci. 18 (4), 820–828. https://doi.org/10.1046/j.1460-9568.2003.02815.x.

Riban, V., Bouilleret, V., Pham-Lê, B.T., Fritschy, J.M., Marescaux, C., Depaulis, A., 2002. Evolution of hippocampal epileptic activity during the development of hippocampal sclerosis in a mouse model of temporal lobe epilepsy. Neuroscience 112 (1), 101–111. https://doi.org/10.1016/S0306-4522(02)00064-7.

Scharfman, H.E., 2019. Current review the dentate gyrus and temporal lobe epilepsy: an 'Exciting' era. Epilepsy Current 19 (4), 249–255. https://doi.org/10.1177/1535759719855952.

Schindler, C.W., Karcz-Kubicha, M., Thorndike, E.B., Müller, C.E., Tella, S.R., Ferré, S., et al., 2005. Role of central and peripheral adenosine receptors in the cardiovascular responses to intraperitoneal injections of adenosine A 1 and A 2A subtype receptor agonists. Br. J. Pharmacol. 144 (5), 642–650. https://doi.org/10.1038/sj.bjp.0706043.

Schmidt-Hieber, C., Jones, P., Bischofberger, J., 2004. Enhanced synaptic plasticity in newly generated granule cells of the adult hippocampus. Nature 429 (6988), 184–187. https://doi.org/10.1038/nature02553.

Somjen, G.G., 2002. Ion regulation in the brain: implications for pathophysiology. Neuroscientist 8 (3), 254–267. https://doi.org/10.1177/1073858402008003011.

Spanoghe, J., Larsen, L.E., Craey, E., Manzella, S., Van Dycke, A., Boon, P., et al., 2021. The signaling pathways involved in the anticonvulsive effects of the adenosine a1 receptor. Int. J. Mol. Sci. 22 (1), 1–26. https://doi.org/10.3390/IJMS22010320.

Spanoghe, J., Wynendaele, E., Vergaelen, M., De Colvenaer, M., Mariman, T., Vonck, K., et al., 2025. Photopharmacological activation of adenosine A1 receptor signaling

suppresses seizures in a mouse model for temporal lobe epilepsy. J. Contr. Release 381, 113626. https://doi.org/10.1016/j.jconrel.2025.113626.
Staley, K.J., Otis, T.S., Mody, I., 1992. Membrane properties of dentate gyrus granule cells: comparison of sharp microelectrode and whole-cell recordings. J. Neurophysiol. https://doi.org/10.1152/jn.1992.67.5.1346.
Strange, B.A., Witter, M.P., Lein, E.S., Moser, E.I., 2014. Functional organization of the hippocampal longitudinal axis, 15. https://doi.org/10.1038/nrn3785.
Tchekalarova, J., Sotiriou, E., Georgiev, V., Kostopoulos, G., Angelatou, F., 2005. Up-regulation of adenosine A1 receptor binding in pentylenetetrazol kindling in mice: effects of angiotensin IV. Brain Res. https://doi.org/10.1016/j.brainres.2004.11.004.
Tescarollo, F.C., Rombo, D.M., DeLiberto, L.K., Fedele, D.E., Alharfoush, E., Tomé, Â.R., et al., 2020. Role of adenosine in epilepsy and seizures. J. Caffeine Adenosine Res. 10 (2), 45–60. https://doi.org/10.1089/caff.2019.0022.
Trinka, E., Cock, H., Hesdorffer, D., Rossetti, A.O., Scheffer, I.E., Shinnar, S., et al., 2015. A definition and classification of status epilepticus–Report of the ILAE task force on classification of status epilepticus. Epilepsia 56 (10), 1515–1523. https://doi.org/10.1111/epi.13121.
Vergaelen, M., Manzella, S., Vonck, K., Craey, E., Spanoghe, J., Sprengers, M., et al., 2024. Increased dentate gyrus excitability in the intrahippocampal kainic acid mouse model for temporal lobe epilepsy. Int. J. Mol. Sci. 25 (1). https://doi.org/10.3390/ijms25010660.
Weltha, L., Reemmer, J., Boison, D., 2019. The role of adenosine in epilepsy. Brain Res. Bull. 151, 46–54. https://doi.org/10.1016/j.brainresbull.2018.11.008.